Physical theory of biological noise buffering by multicomponent phase separation

Dan Deviri[a,1] and Samuel A. Safran[a]

[a]Department of Chemical and Biological Physics, Weizmann Institute of Science, Rehovet 76100, Israel

Edited by Daan Frenkel, University of Cambridge, Cambridge, United Kingdom, and approved May 19, 2021 (received for review January 4, 2021)

Maintaining homeostasis is a fundamental characteristic of living systems. In cells, this is contributed to by the assembly of biochemically distinct organelles, many of which are not membrane bound but form by the physical process of liquid–liquid phase separation (LLPS). By analogy with LLPS in binary solutions, cellular LLPS was hypothesized to contribute to homeostasis by facilitating "concentration buffering," which renders the local protein concentration within the organelle robust to global variations in the average cellular concentration (e.g., due to expression noise). Interestingly, concentration buffering was experimentally measured in vivo in a simple organelle with a single solute, while it was observed not to be obeyed in one with several solutes. Here, we formulate theoretically and solve analytically a physical model of LLPS in a ternary solution of two solutes (ϕ and ψ) that interact both homotypically (ϕ–ϕ attractions) and heterotypically (ϕ–ψ attractions). Our physical theory predicts how the coexisting concentrations in LLPS are related to expression noise and thus, generalizes the concept of concentration buffering to multicomponent systems. This allows us to reconcile the seemingly contradictory experimental observations. Furthermore, we predict that incremental changes of the homotypic and heterotypic interactions among the molecules that undergo LLPS, such as those that are caused by mutations in the genes encoding the proteins, may increase the efficiency of concentration buffering of a given system. Thus, we hypothesize that evolution may optimize concentration buffering as an efficient mechanism to maintain LLPS homeostasis and suggest experimental approaches to test this in different systems.

phase separation | out-of-equilibrium thermodynamics | biological noise | soft matter | biological physics

Over the past decade, a significant body of research has revealed the crucial involvement of liquid–liquid phase separation (LLPS) in the formation of many membraneless organelles, also known as biomolecular condensates (BMCs) (1), among which are the nucleolus (2), P granules (3), stress granules (4), and heterochromatin (5). The distinct biochemical environment of the BMCs (e.g., enzymes, substrates) can promote reactions related to important biological functions. This property is similar to membrane-bound organelles. However, in contrast to membrane-bound organelles, whose homeostasis is maintained by the out-of-equilibrium action of active pumps and channels embedded in the membrane, the concentration homeostasis in BMCs is established due to attractive interactions among molecules and the solution entropy of the phase-separating components. In several situations, such as those of the different types of ribonucleoprotein bodies (6), the BMCs are formed in systems with two or more solutes. For the situation of two solutes with interactions that dominate the mixing tendency of the entropy (proportional to the temperature), one can think of two simple limits. Attraction between molecules of one species (homotypic) leads to segregative LLPS where the other solute is mostly excluded from the BMCs, while attraction between molecules of different types (heterotypic) leads to associative LLPS where both solutes cooperatively form BMCs (Fig. 1) (7). In the more realistic case, combinations of homotypic and heterotypic attractions can drive diverse types of LLPS, leading to a rich variety of BMCs that may themselves consist of multiple phases, such as the layered nucleolus (2). In this work, if not specified otherwise we consider LLPS into two phases, which gives rise to one phase that is a BMC that thermodynamically coexists with a phase that is (much) more dilute in the solute concentrations.

The large number of BMCs and apparent ubiquity of LLPS as an organizational principle of organelles in living cells suggest that it confers some evolutionary advantages. One of the hypothesized advantages is mitigating the deleterious outcomes of "expression noise" (1). Cells, even when carrying identical genomes, exhibit natural variations of the concentrations of proteins and RNA molecules within them, which when measured in an ensemble of genetically identical cells, follow a statistical distribution rather than deterministic values (8). These variations are known as expression noise and originate from two biophysical causes. The first is the fluctuations in expression rates of genes, primarily due to stochastic changes of the transcriptional activity of genes, known as transcriptional bursting (9). The contribution to the variations of protein and RNA concentrations due to intrinsic fluctuations of their expression rates is known as "intrinsic noise," which is uncorrelated among different genes (10). The second, known as "extrinsic noise," is due to variations of the concentrations of associated molecules related to transcription and translation, such as transcription factors, polymerases, or ribosomes; this is due to intrinsic noise in the expression rates of those associated molecules. Such variations can affect the expression rates of multiple genes in a correlated manner (10). For biochemical processes that require a narrow concentration range

Significance

The stochastic nature of transcription/translation implies that the concentrations of cellular proteins are "noisy" and not constant in time or across cell populations. Liquid–liquid phase separation (LLPS) can reduce or "buffer" this noise by maintaining well-defined concentrations, even in the presence of concentration distributions. However, this idea was recently challenged experimentally in multicomponent systems. Our physical theory of LLPS in ternary systems (solutes ϕ and ψ in a solvent) predicts their LLPS properties as a function of the ϕ–ϕ (homotypic) and ϕ–ψ (heterotypic) interaction strengths. We show how buffering can be effective if the noise distribution aligns with the tie-lines of the phase diagram and suggest that evolution may optimize concentration buffering by selecting appropriate mutations.

Author contributions: D.D. and S.A.S. designed research, performed research, and wrote the paper.

The authors declare no competing interest.

This article is a PNAS Direct Submission.

Published under the PNAS license.

[1]To whom correspondence may be addressed. Email: dan.deviri@weizmann.ac.il.

This article contains supporting information online at https://www.pnas.org/lookup/suppl/doi:10.1073/pnas.2100099118/-/DCSupplemental.

Published June 16, 2021.

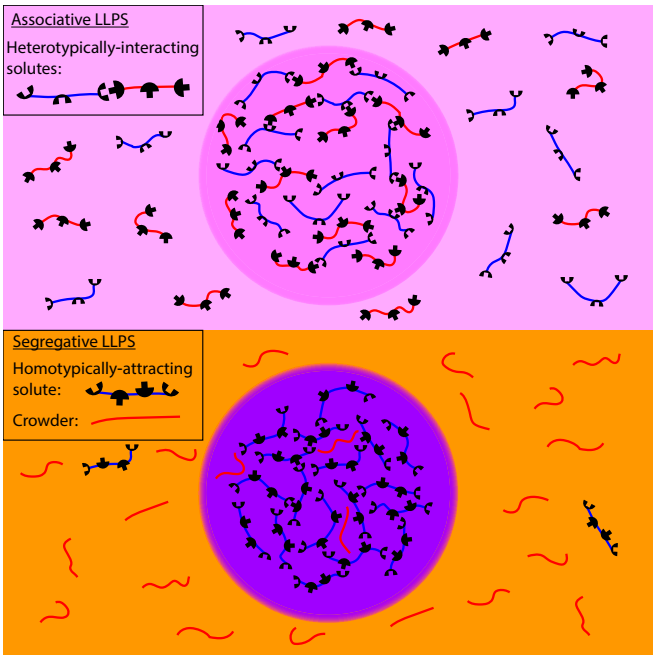

Fig. 1. Illustration of associative vs. segregative LLPS. (*Upper*) Two types of solute molecules (red and blue) that interact heterotypically (attractions of blue and red) undergo associative LLPS and form a dense phase rich in both solutes (light purple) that coexist with a solution dilute in both solutes (light pink). (*Lower*) A homotypically attractive solute (where blue attracts blue) and an inert "crowder" (red) undergo segregative LLPS and form a phase rich in the attractive solute but poor in the crowder (purple) and a phase rich in crowder but poor in attractive solute (light orange).

of molecules to be faithfully executed, expression noise can be detrimental (11).

LLPS may mitigate the harmful effects of expression noise by facilitating "concentration buffering." Fluctuations in the overall (spatially averaged) concentrations of the molecules are "buffered" (shielded), so that all of the changes in the overall concentrations are merely absorbed in changes of the volumes of the phases, while the concentrations of the molecules within each phase remain unchanged at fixed equilibrium values. This allows the biological function of the BMCs, which may be sensitive to the concentrations, to remain robust to their stochastic fluctuations (1, 12, 13). This "simplistic" type of concentration buffering exists only in equilibrium LLPS of binary solutions, consisting of a single solute in a solvent, where the solute concentrations in the two coexisting phases are determined by the interaction energy and temperature, independent of the overall concentration of the solute (14); the latter only fixes the relative volumes of the two phases. Nonetheless, in the multicomponent, out-of-equilibrium cellular environment, a recent experimental study has demonstrated that, in the context of LLPS driven by homotypic interactions among a single peptide species (15), concentration buffering may decrease concentration fluctuations at the scale of the BMC domains (whose sizes are ∼100 nm to 1 μm). In contrast, multiple studies, both in vivo and in vitro, focusing on LLPS that is driven by a combination of heterotypic and homotypic interactions among multiple types of solutes have observed changes of protein concentrations within different phases as the overall protein concentrations were varied (16–19). At first glance, this shows the lack of concentration buffering in multicomponent systems in which heterotypic interactions contribute to LLPS.

To resolve this puzzle, in this paper, we theoretically demonstrate how concentration buffering is nevertheless maintained in multicomponent solutions with both homotypic and heterotypic interactions. We focus on a specific example of the case of two solutes in a solvent (ternary system) that can form either segregative or associative phase-separated volumes. The buffering is more subtle and constrained than in the simplistic case but can nonetheless be effective, depending on the correlations of the noise affecting the expression of the two components as we predict. Notably, LLPS of ternary polymer–polymer–solvent systems has been extensively researched in the past (for example, refs. 20–22); however, these previous works did not consider the buffering of biological noise in such systems, which is the focus of this paper.

As we explain in *Concentration Buffering in Solutions of Two Solutes*, despite this general dependence in multicomponent LLPS, there is always a special, correlated change of the overall concentrations that nevertheless does not change the coexisting concentrations. If the expression noise of multiple genes that encode the molecular components of the phase-separating system is correlated by the underlying gene network in a manner similar to the lines (*Concentration Buffering in Solutions of Two Solutes*), its effect on the coexisting concentrations is buffered. We hypothesize that, for the biological contexts in which expression noise is deleterious, such matching might be subject to evolutionary pressure. We elaborate upon this in a pictorial manner in the next section and quantify and classify in a generic manner the relevant phase diagrams for different relative magnitudes of homotypic and heterotypic interactions in *Results*. This is preceded by a section that introduces our model, which treats in a unified manner LLPS driven by both homotypic and heterotypic interactions.

In *Discussion*, we delineate scenarios in which the correlations of the expression noise may lead to effective noise buffering. As an example, based on the regulatory network associated with the proteins involved, the outer layer of the nucleolus may be an example of such a match. In addition, we suggest future experiments required to further test our evolutionary hypothesis and discuss the possible evolutionary mechanisms that contribute to buffering. Surprisingly, our model predicts that under certain conditions, archetypical solutions of multivalent scaffold and multivalent binding partner can exhibit reentrant LLPS as the heterotypic interaction strength is varied, a prediction that is qualitatively supported by recent experimental observations (23). In addition, we discuss how concentration buffering can be generalized from a three-component system to a system with a larger number of components that phase separate into multiple phases. We predict that in such cases the buffering becomes more effective as the number of equilibrium phases increases.

Concentration Buffering in Solutions of Two Solutes

While the phenomenon of LLPS of equilibrium solutions with a single solute inspired the notion of concentration buffering (1), the situation in the case of cellular LLPS is more complex due to two major reasons. 1) The cellular environment is an aqueous solution that contains many species of solutes, rather than a single solute as in binary solutions. 2) Within the cellular environment, proteins and RNA molecules are dynamically produced and degraded, in contrast to the equilibrium solutions where the overall solute concentration is fixed.

We first address point 1 and clarify the qualitative differences between LLPS of multisolute and of single-solute solutions via examination of a ternary system with two solutes. While phase diagrams (for constant interaction strengths) of binary systems are two-dimensional (2D; temperature vs. solute concentration), those of ternary systems are three-dimensional (3D; temperature vs. the concentrations of the two solutes). However, since the temperature in cellular systems is usually constant, the coexisting concentrations of a phase-separated system are described by a "slice" of the phase diagram, taken at constant temperature.

For a binary system, the result is one-dimensional and determines two unique coexisting concentrations for each temperature. However, in ternary systems the constant temperature slice is 2D and results in a multitude of coexisting concentrations, given by the binodal curve that separates the one-phase region from the two-phase region in the concentration–concentration phase diagram (Fig. 2*A*). In contrast to the unique concentration buffering in single-solute systems, for LLPS of solutions with two (or more) solutes, buffering is incomplete since the two coexisting concentrations of solutes can vary with the overall concentrations (16). Nevertheless, there are directions in the 2D concentration–concentration phase diagram of the ternary system, along which concentration buffering can be uniquely defined: namely, the directions of the tie-lines, defined as lines that connect pairs of coexisting concentrations in the concentration–concentration phase diagrams. The variation of overall concentration along the tie-lines always results in coexisting phases with the same concentrations (buffering); variations in the overall concentrations only modify the relative volumes of the two coexisting phases. However, variations of the overall concentrations that deviate from a tie-line result in changes of the coexisting concentrations (Fig. 2*A*).

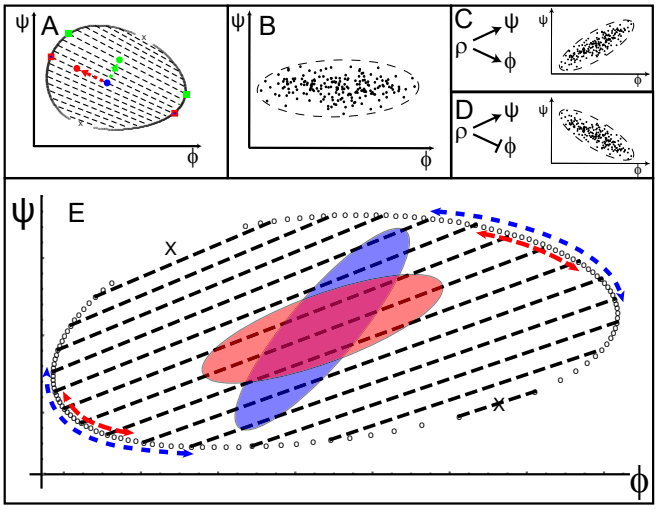

Fig. 2. Biological noise and concentration buffering. (*A*) Consequences of variations in the overall concentrations (shown as full circles) on the steady-state concentrations of each of the solutes in the two coexisting phases (full squares) along and perpendicular to the tie-lines (black dashed lines). A variation of the initial concentrations of the two solutes represented by the blue circle along the direction of the red arrow, which is aligned with the tie-line, does not change the coexisting concentrations (red squares with blue dots in the center). In contrast, a variation of the same initial concentrations in the direction of the green arrow perpendicular to the tie-line changes the coexisting concentrations, which now have the values indicated by the green squares. (*B*) A significant part of the distribution of the overall concentrations and its envelope, the noise ellipse, when only intrinsic noise is present. The intrinsic noise in the expression of solute ϕ is more prominent, so that the major axis of the noise ellipse is parallel to the ϕ axis. (*C* and *D*) Tilted noise ellipses in the presence of both intrinsic and extrinsic noises; the latter originates from concentration fluctuations of a common transcription factor ρ. In *C*, ρ induces the expression of both ϕ and ψ, while in *D*, it induces ψ and represses ϕ. (*E*) The relation between the alignment of the tie-lines (dashed black lines) and the orientations of the noise ellipses (blue and red ellipses) determines the degree of concentration buffering. The axes of the two noise ellipses are equal in length; however, the direction of the red ellipse is aligned with the direction of the tie-lines, while the direction of the blue ellipse is not. Variations in the concentrations of the two solutes in the coexisting phases (dashed blue arrows) due to the blue noise ellipse are significantly larger than the variations in the coexisting concentrations (marked by the red arrows) due to the red noise ellipse.

We now address point 2, and we discuss the time-dependent effect of biological noise that results in variations of the overall protein concentrations in the cell and relate this to the buffering along sets of tie-lines in two-solute systems. We first investigate how the nonequilibrium production and degradation of solutes change the nature of phase separation compared with equilibrium, and then, we analyze how the concentration fluctuations are represented in the phase diagram and modify the coexisting concentrations. We theoretically address these two questions in *SI Appendix*, section 1. Below, we relate the outcome of this theory to concentration buffering for solutions with two solutes.

The biological noise in the cell is caused by fluctuations of the production and degradation rates of various proteins and RNA molecules. Even in the case that there is no production noise, the timescales of protein and RNA degradation are of the order of hours (24), while the timescale for diffusion of proteins and RNA molecules, which determines the dynamics of demixing, is of the order of seconds (24). This separation of timescales gives rise (*SI Appendix*) to steady-state, nonequilibrium coexisting concentrations that are almost the same as those described by equilibrium phase diagrams. Moreover, this separation of timescales implies that the lengths that solute molecules traverse before they are degraded are much larger than the length scales associated with the short-range interactions that lead to LLPS. At the mesoscale (micrometers), the long length scales traversed by the solutes before they are degraded do affect the spatial distribution of the domains of dense and dilute phases. While in equilibrium LLPS, the concentrated domains undergo coarsening that eventually results in a single domain (25), in nonequilibrium LLPS, this is not the case, similar to other nonequilibrium systems such as active emulsions (26, 27). We show in *SI Appendix* that in steady state, spatially uniform solute production results in finite-sized 3D domains. We determine their size in agreement with other theoretical work (28). In the case that the production is localized to a small number of regions, there may be multiple concentrated domains or even aspherical ones, in agreement with the measurements and numerical model of ref. 29. Only when the production is localized to a single small region does our theory predict a single spherical, concentrated domain as in equilibrium LLPS.

In addition to the separation of timescales between diffusion and degradation, the timescales that are associated with fluctuations of the production rate (due to biological noise) and demixing are also well separated. The former [of the order of hours (9)] is much slower than the latter [of the order of seconds (24)]. This implies that during the formation of BMCs by LLPS, the rate of production hardly changes. Therefore, the steady-state solute concentrations in the BMCs and their coexisting environment are determined as if the production and degradation were constant in time but quasistatically follow the slow changes in production rate. Thus, the probability distribution of overall concentrations that result from the biological noise can be simply superimposed on the phase diagram. The variation of the coexisting solute concentrations is determined by the projections of the distribution of overall concentrations along the tie-lines on the binodal.

In *SI Appendix*, we derive the shape of this distribution (defined as the contour of constant probability density that is $1/e^2$ of its maximal value) from linear response theory for small fluctuations that are uncorrelated in time. We predict that the noise-induced distribution is, in general, a tilted ellipse centered at solute concentrations determined by the average production and degradation rates. We determine the lengths of the axes of this "noise ellipse" and its orientation as functions of the magnitudes of both the extrinsic and intrinsic types of biological noise

involved in gene expression (8, 10). We show that for a system of two solutes with only intrinsic noise, the axes of the noise ellipse are parallel to the two axes of the solute concentrations (Fig. 2*B*). However, the presence of the extrinsic noise whose effects on the expression of the two genes are correlated rotates the noise ellipse and allows it to obtain any orientation within the phase diagram (Fig. 2 *C* and *D*).

In the case that the major axis of the noise ellipse is aligned with the tie-lines, the main effect of the noise is to shift the concentrations of the two solutes along the tie-lines, so that the resulting coexisting concentrations of the two coexisting phases remain fixed, independent of the noise (i.e., the system shows concentration buffering). Of course, the noise in the direction of the minor axis does contribute to variations of the coexisting concentrations. The length of the minor axis is minimal when the extrinsic noise is zero, so that the variations in coexisting concentrations that are attributed to the intrinsic noise present a lower bound to the efficacy of concentration buffering; however, if this intrinsic noise is small, the variations of the two coexisting phases will be small, when concentration buffering is optimal. As shown in Fig. 2*E*, concentration buffering may thus reduce the noise in a multicomponent solution with increasing efficiency as the orientations of the noise ellipse and the tie-lines of the phase diagram become more aligned. If biological noise decreases the fitness of the organism (11), alignment of the major axis of the noise ellipse and the tie-lines may be an evolutionary optimized fitness criterion.

We note that a more realistic noise structure, such as the one that originates from transcriptional bursting, may modify the shape of the noise ellipse. However, as long as the noise affecting the two genes is correlated (so that the distribution is not circularly symmetric) and the timescales associated with it are longer than those of diffusion, the distribution can be superimposed on the phase diagram so that the hypothesis regarding the alignment of the distribution with the tie-lines is valid. The orientation of the tie-lines depends on several generic features of the intermolecular interactions, which as explained above, can be predicted using the theory of equilibrium LLPS. We present a model that allows us to predict the phase diagrams and tie-line orientations for three archetypical cases in the following section.

Theoretical Model of Multicomponent LLPS

In this section, we present a physiochemical model that predicts the phase diagrams and tie-lines for ternary systems. This allows us to predict the generic features of the phase diagrams that are relevant to the problem of concentration buffering. The free energy of our model, which is a three-component generalization of the Flory Huggins (FH) model, takes into account both homotypic and heterotypic interactions and allows us to investigate their distinct effects on the LLPS properties of the solution in *Results*. Gradient terms in the free energy give rise to interfacial energy that modifies the size and shapes of the phase-separated domains but do not affect the concentration of solutes within these domain (*SI Appendix*, section 1); thus, they are not included below. The generalization of this approach to systems with more than two solutes is discussed in *SI Appendix*.

The two solutes interact via short-range interactions (e.g., proteins in the cytoplasm), and we write an approximate mean-field expression for the free energy that includes both the entropy of mixing and interaction energies. The free energy density $f(\phi,\psi)$ is a function of the local volume fractions of the two solutes ϕ,ψ; the volume fraction of solvent ϕ_s (for a system of incompressible molecules) is then fixed at $\phi_s = 1-(\phi+\psi)$. The function $f(\phi,\psi)$ contains all of the information needed to characterize the equilibrium state of the system, which minimizes the total free energy of the system, subject to the constraint that the total numbers of molecules of each type are conserved. These imply (14) that, in equilibrium, the free energy change resulting from the addition or removal of a molecule of any type from each phase, known as its chemical potential, must be the same in each of the coexisting phases. If the chemical potentials for the different phases are different, the free energy is not minimal because a nonequilibrium flux of molecules from a phase of high chemical potential to a phase of low chemical potential decreases the total free energy. Next, the equilibrium free energy change resulting from an increase or decrease of the volume of each of the coexisting phases, known as its osmotic pressure, must also be the same in each phase. Similar to the case of chemical potentials, an imbalance of the osmotic pressures results in a nonequilibrium expansion of the high-pressure phase at the expense of the low-pressure phase (i.e., resulting from a flux of solvent molecules); this would decrease the total free energy of the system, indicating that the total free energy is not minimal. The conditions of equality of chemical potentials and the osmotic pressures are expressed, in terms of the free energy density f, as the following equations for two-phase equilibria (*SI Appendix*):

$$0 = \frac{\partial f(\phi_i,\psi_i)}{\partial \phi_i} - \frac{\eta_\phi}{v_0} \quad [1]$$

$$0 = \frac{\partial f(\phi_i,\psi_i)}{\partial \psi_i} - \frac{\eta_\psi}{v_0} \quad [2]$$

$$0 = f(\phi_i,\psi_i)v_0 - \eta_\phi\phi_i - \eta_\psi\psi_i + \pi, \quad [3]$$

where v_0 is a molecular volume of the order of the volume of a segment of the polymers (both ϕ and ψ) that is of the length of one persistence length; ϕ_i and ψ_i are the concentrations (in terms of volume fractions) of the solute molecules ϕ and ψ, respectively, in phase i, where $i=1,2$; η_ϕ and η_ψ are the chemical potentials of solutes ϕ and ψ, respectively; and π is the osmotic pressure of the phases. In *SI Appendix*, we generalize this to systems with more than two solutes and two equilibrium phases and also show how the thermodynamic equilibrium conditions dictate the volumes and concentrations of molecules of each type in the coexisting phases.

To predict the phase diagrams of biological systems, we must specialize the model to the situation of LLPS of biomolecules. In biological systems, the majority of the phase-separating molecules are multivalent intrinsically disordered proteins (IDPs) and RNA molecules (30). These molecules are usually described as a collection of different "stickers" connected by "spacers" (e.g., polymeric backbone), where a group of stickers of specific types may interact strongly (30). Homotypic interactions refer to stickers belonging to the same type of molecules, while heterotypic interactions refer to stickers belonging to molecules of different types. Molecules that contain different kinds of stickers may potentially interact both homotypically and heterotypically. In solutions, most IDPs and RNA molecules usually appear as open, unstructured coils rather than compact globules (31, 32). Therefore, stickers and spacers of different molecules are accessible to each other and may interact. As an approximation, we follow the FH model in which all of the monomeric segments uniformly contribute to the interactions, regardless of their position along the polymer backbone. This is different from compact objects, such as globular proteins, whose surface amino acids are the only ones that participate in intermolecular interactions; in that case, the mean-field treatment of FH theory may be inappropriate (33). However, such globular proteins are less prone to phase separate compared with IDP (1). Presumably, this is due to the smaller fraction of amino acids of globular proteins that can participate in intermolecular interactions compared with IDPs.

For a ternary solution comprising two solutes in a solvent, the free energy density f in the FH theory is written as (*SI Appendix* has details)

$$f(\phi,\psi)v_0 = \frac{\phi}{N_\phi}\log(\phi) + \frac{\psi}{N_\psi}\log(\psi) + (1-\phi-\psi) \times \log(1-\phi-\psi) - \frac{1}{2}\chi_{\phi\phi}\phi^2 - \chi_{\phi\psi}\phi\psi - \frac{1}{2}\chi_{\psi\psi}\psi^2, \quad [4]$$

where ϕ and ψ are the concentrations of the two polymers, N_ϕ and N_ψ are the numbers of persistence lengths (34) of each polymer and the set of $\{\chi_{ij}\}$ are the FH interaction parameters, with $\chi_{\phi\phi}$ and $\chi_{\psi\psi}$ accounting for the homotypic (self-attractive) interaction energies of monomers of type ϕ and ψ, respectively, while $\chi_{\phi\psi}$ is the heterotypic interaction energy related to attractive interactions between the monomers of the two different types, ϕ and ψ. We use the convention in which all of the energies are divided by the thermal energy $k_B T$ and hence, are dimensionless. Importantly, the solvent molecules are not necessarily the size of one persistence length (*SI Appendix* has details).

We note that FH models with a single interaction parameter for every pair of molecule type, which averages the relevant stickers over the entire polymer, have been shown to approximate well the LLPS properties of heterogeneous stickers-and-spacers proteins in both experimental (16) and theoretical (35) contexts. We next use Eqs. **1–3** to plot the phase diagrams and tie-lines for concrete examples of biological interest.

Results

Most BMCs consist of a single phase with a relatively high concentration of multiple protein species, which coexists with an aqueous phase where these proteins are dilute (36). This coexistence results from LLPS that forms two phases. To focus on LLPS that give rise to two-phase equilibria, we consider ternary solutions in which one of the solutes, ψ, has no homotypic attraction by setting $\chi_{\psi\psi}=0$. Indeed, as detailed in the subsections below, we find that ternary solutions with $\chi_{\psi\psi}=0$ can phase separate into only two phases. In *SI Appendix*, we discuss the scenario of LLPS of solutions with more than two solutes that phase separate into more than two phases, which may provide an even more robust concentration buffering.

When $\chi_{\psi\psi}=0$, there are three archetypical combinations of the homotypic interaction parameter $\chi_{\phi\phi}$ and the heterotypic one $\chi_{\phi\psi}$: 1) $\chi_{\phi\phi}>0$ and $\chi_{\phi\psi}=0$, in which ϕ can phase separate into a phase with a relatively high concentration of ϕ that coexists with an aqueous phase that also contains ψ; 2) $\chi_{\phi\phi}=0$ and $\chi_{\phi\psi}>0$, in which neither ϕ nor ψ separately phase separate into a relatively high-concentration phase but can phase separate into a phase that contains a relatively high concentration of them both, due to the heterotypic interactions; and 3) $\chi_{\phi\phi}>0$ and $\chi_{\phi\psi}>0$, which combine the two former cases. In this scenario, the presence of both homotypic and heterotypic interactions can drive LLPS with relatively high concentrations of both molecules or a phase with a relatively high-concentration phase of only one of them, depending on the relative strengths of the two interactions. Each of these cases is analyzed below, and the appropriate phase diagrams are plotted using Eq. **4** for the free energy with the relevant interaction parameters. Eqs. **1–3** are then used to predict the binodal and tie-lines, respectively defined as the curve that separates the one-phase region from the two-phase region and the lines connecting pairs of coexisting concentrations. To find the critical points, which are points in concentration space in which the compositions of the two coexisting phases are identical, we followed the method presented in the third section of the supplemental information in ref. 37.

Importantly, the interaction energies we choose to generate the phase diagrams presented in this section are intentionally low. This is because we wish to obtain binodal curves whose dependence on the concentrations can be visually resolved in a linear–linear plot. Such low interaction energies result in concentrations in the dilute phase that are larger than those observed in vivo. An increase of the relevant interaction energies exponentially rescales and significantly reduces the solute concentrations in the dilute phases (37), so that our theory can account for the concentrations that are observed in vivo. However, such concentration ranges necessitate the use of a log–log plot in which the tie-lines are not straight, so that the notion of their orientation is lost, which makes it undesirable for the purpose of our paper.

Case I—Homotypic ($\chi_{\phi\phi}>0, \chi_{\phi\psi}=0$): Concentrated Phase Rich in One Solute (Segregative LLPS). Biological environments such as the cytoplasm contain a large number of macromolecules that do not significantly or specifically interact with proteins that undergo homotypic LLPS but of course, cannot occupy the same location in space as the other proteins or solvent molecules (excluded volume interactions); such macromolecules are referred to as crowders. Excluded volume interactions introduced by crowders are inherently accounted for in FH theory by its construction. Thus, we model crowding by considering one solute ϕ with homotypic (self-attractive) interactions $\chi_{\phi\phi}>0$ and another, ψ (the crowder), that interacts attractively neither with ϕ nor with itself ($\chi_{\phi\psi}=\chi_{\psi\psi}=0$).

In Fig. 3, we plot two concentration–concentration phase diagrams for this case, calculated using typical homotypic interaction strengths. We identify three classes of phase diagrams. The first type, presented in Fig. 3*A*, is the one in which the binodal intersects the $\psi=0$ axis, indicating that the solute ϕ can phase separate even in the absence of crowder solutes. The quantitative ranges of the molecular interactions and sizes for which this occurs are determined by the condition $\chi_{\phi\phi}>\chi^c_{\phi\phi}$, whose dependence on the interactions and molecular lengths is given in *SI Appendix*, as it is for all of the other critical values of interaction parameters; the characteristic values of the interaction parameters and the topological properties of the phase diagrams that are associated with them are listed in *SI Appendix*, Tables S1 and S2. The second type, presented in Fig. 3*B*, is the one in which the binodal does not intersect the $\psi=0$ axis, indicating that crowding is required for LLPS of solute ϕ. This type is characterized by interaction energies in the range $\chi^c_{\phi\phi}>\chi_{\phi\phi}>\chi^m_{\phi\phi}$ (*SI Appendix*). The third type of phase diagram, which we do not plot, is one in which LLPS does not occur and the single-phase, homogenous solution is the equilibrium state for all concentrations ϕ,ψ (*SI Appendix*). This happens when the homotypic interaction is smaller than another critical value, $\chi_{\phi\phi}<\chi^m_{\phi\phi}$ (*SI Appendix*). In the phase diagrams of Case I, the tie-lines connecting coexisting pairs of concentrations generally have negative slope, indicating that the LLPS is segregative, namely one of the phases is rich in the homotypically attracting solute and poor in the crowder and the other is poor in the homotypically attracting solute and rich in the crowder.

Case II—Heterotypic ($\chi_{\phi\phi}=0, \chi_{\phi\psi}>0$): Concentrated Phase Rich in Both Solutes (Associative LLPS). For some BMCs, LLPS is the result of heterotypic interactions between molecules of different types, which have only negligible homotypic interactions, so that they do not undergo LLPS when separately mixed with solvent. In the context of our model, we set $\chi_{\phi\phi}=\chi_{\psi\psi}=0$ while keeping $\chi_{\phi\psi}>0$ to predict the resulting phase diagrams of such systems (Fig. 4).

The binodals for different values of the heterotypic interactions, $\chi_{\phi\psi}$, form closed loops. The physical interpretation of the loops is that they represent a certain region of "stoichiometric" ratios of the two solutes that interact in a heterotypic manner and strongly enough to phase separate from the aqueous phase (39). Within these loops, the tie-lines have positive slopes, indicating

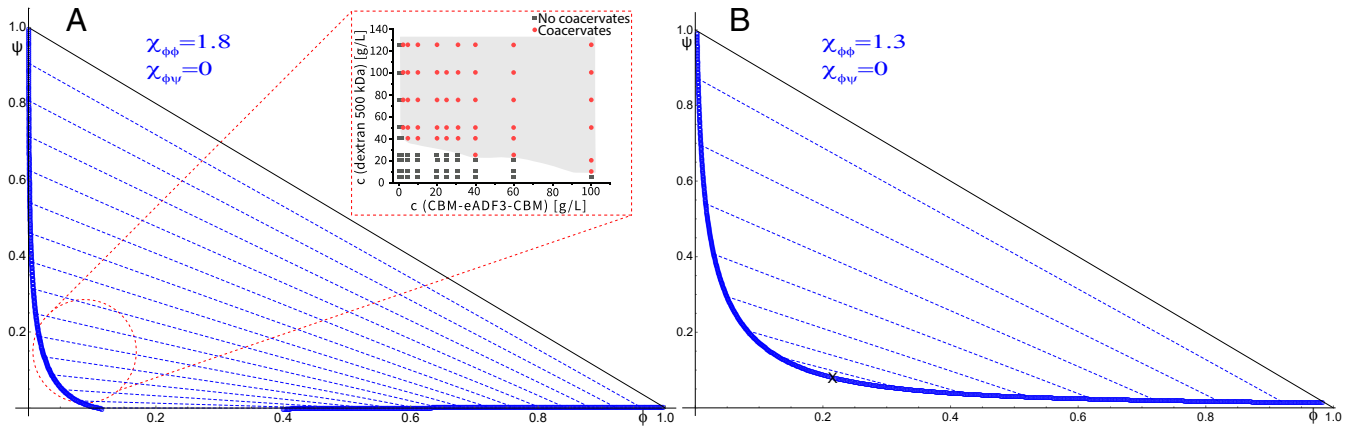

Fig. 3. Typical phase diagrams of a ternary system with a homotypically attracting solute ϕ and a crowder ψ (where $\chi_{\phi\psi} = 0$ and $\chi_{\psi\psi} = 0$). Binodals are marked by blue open circles (that sometimes coalesce and appear as solid lines), tie-lines are marked by blue dashed lines, and critical points are marked with X marks. (*A*) Phase diagram for $N_\phi = 10$, $N_\psi = 6$, and $\chi_{\phi\phi} = 1.8$, which is larger than the critical value $\chi^c_{\phi\phi} \approx 1.73$ (*SI Appendix*) required for phase separation in the absence of the crowder. The binodal intersects the line $\psi = 0$, indicating that the solute ϕ can phase separate even in the absence of the crowder, ψ. However, the presence of crowders ($\psi > 0$) increases the concentration of ϕ in the dense phase and decreases it in the dilute phase. (*Inset*) In vitro measurements of an experimental phase diagram of such a ternary system containing a homotypically-attracting triblock protein based on engineered spidroin-like protein (CBM-eADF3-CBM), a crowder (dextran), and an aqueous solvent. The measured phase diagram shows the same trend as the one we predict in the region enclosed in the red dashed circle. Adapted from figure 2 in ref. 38. (*B*) Phase diagram for $N_\phi = 10$, $N_\psi = 6$, and $\chi_{\phi\phi} = 1.3$, which is less than the critical value $\chi^c_{\phi\phi}$ for phase separation in the absence of crowder but greater than $\chi^m_{\phi\phi}$, below which the homotypically attracting solute cannot phase separate even in the presence of crowders (*SI Appendix*). Within this range of homotypic interactions, the binodal does not intersect the line $\psi = 0$, indicating that crowders are necessary to facilitate LLPS of the homotypically attracting solute, ϕ. In both cases, the presence of crowders causes the tie-lines to be negatively sloped, indicating that the LLPS in the presence of crowders is segregative.

that the LLPS is associative; namely, one phase is relatively rich in both solutes, and the other is relatively poor in both but rich in solvent. The area bounded by the loops, which includes the range of protein concentrations that lead to LLPS, shrinks with decreasing $\chi_{\phi\psi}$. Below a critical value of heterotypic interaction energy, $\chi^c_{\phi\psi}$, the binodal disappears, and the homogenous mixed state of the solution becomes the equilibrium state for any concentrations ϕ, ψ. Our model predicts the value of this critical interaction energy as a function of the solute lengths N_ϕ and N_ψ (*SI Appendix*).

Case III—Homotypic and Heterotypic Interactions ($\chi_{\phi\phi} > 0$, $\chi_{\phi\psi} > 0$): LLPS of a Scaffold with a Multivalent Binding Partner. This case accounts for LLPS of multivalent scaffold molecules with homotypic interactions (ϕ), in the presence of multivalent client (binding partner, ψ) molecules that

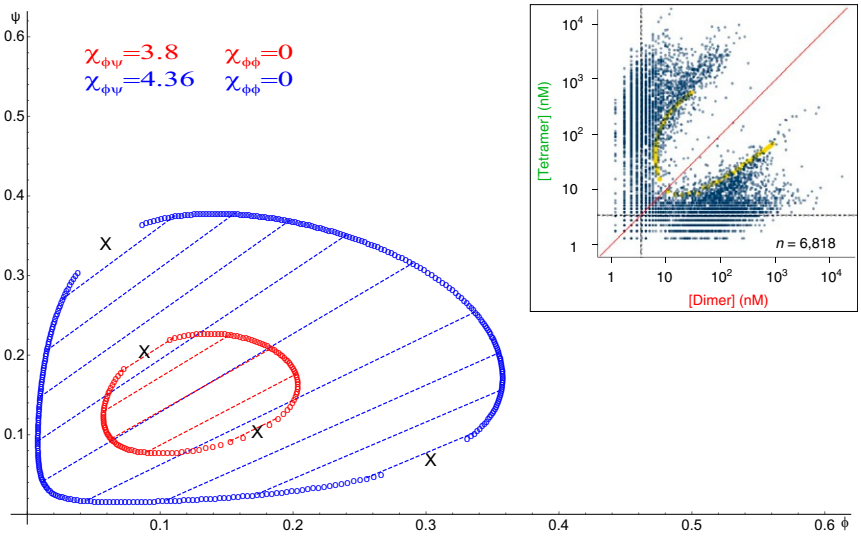

Fig. 4. Typical phase diagrams of ternary systems of two solutes in a solvent that interact purely heterotypically: $\chi_{\phi\psi} > 0$, but $\chi_{\phi\phi}$ and $\chi_{\psi\psi}$ are both zero. Binodals are marked by open circles (that sometimes coalesce and appear as solid lines), tie-lines are marked by dashed lines, and critical points are marked with X marks. The red binodal (and tie-lines) is for $\chi_{\phi\psi} = 3.8$, and the blue is for $\chi_{\phi\psi} = 4.36$. In both cases, $N_\phi = 10$ and $N_\psi = 6$. Systems with weaker heterotypic interactions phase separate with smaller binodal loops in the phase diagram. Both phase diagrams have positively sloped tie-lines, indicating associative LLPS. (*Inset*) An example of an experimentally measured phase diagram of a system of two multivalent molecules (expressed in living cells) that interact heterotypically. The scattered points in the phase diagrams represent the overall concentrations of the two solutes in cells that do not exhibit LLPS. The yellow curve that delineates a region with a lower density of points, namely the two-phase region of the phase diagram, is part of the binodal. The experimental phase diagram shares the same qualitative features of our predicted phase diagram (e.g., shape of the binodal). Adapted from figure 2G in ref. 39.

interact heterotypically with the scaffold molecules but have no homotypic interactions of their own. Within the context of our model of two solutes in a solvent, we set the homotypic interaction of the ψ molecules to 0, $\chi_{\psi\psi}=0$, but keep $\chi_{\phi\phi}, \chi_{\phi\psi} > 0$.

The area of the two-phase region of the resulting phase diagrams, plotted in Fig. 5, shows a surprising, nonmonotonic behavior as the heterotypic interaction parameter is changed. For small heterotypic interactions, the phase diagrams of the scaffold–client model resemble the homotypic phase diagrams of Case I (Fig. 3) with negative-sloped tie-lines. However, as the heterotypic interaction, $\chi_{\phi\psi}$, increases, the binodal shrinks, a larger region of the phase diagram is in the single-phase regime (Fig. 5 *A* and *C*), and the slopes of the tie-lines become less negative.

If the scaffold molecule only phase separates in the presence of a crowder (Case I above), the binodal becomes a loop that shrinks with increasing $\chi_{\phi\psi}$ and eventually disappears (Fig. 5 *A* and *D*) when $\chi_{\phi\psi}$ exceeds a lower critical value, $\chi^{lc}_{\phi\psi}$, that depends on the homotypic interaction and the molecular sizes (*SI Appendix*). Further increase of $\chi_{\phi\psi}$ above an upper critical value, $\chi^{uc}_{\phi\psi}$, which also depends on the homotypic interaction and the molecular sizes (*SI Appendix*), results in reemergence of the binodal as a loop. The reemerging loop expands in size as $\chi_{\phi\psi}$ increases (Fig. 5 *B* and *D*) and has positively sloped tie-lines, similar to Case II of the heterotypic phase diagrams (Fig. 4). For

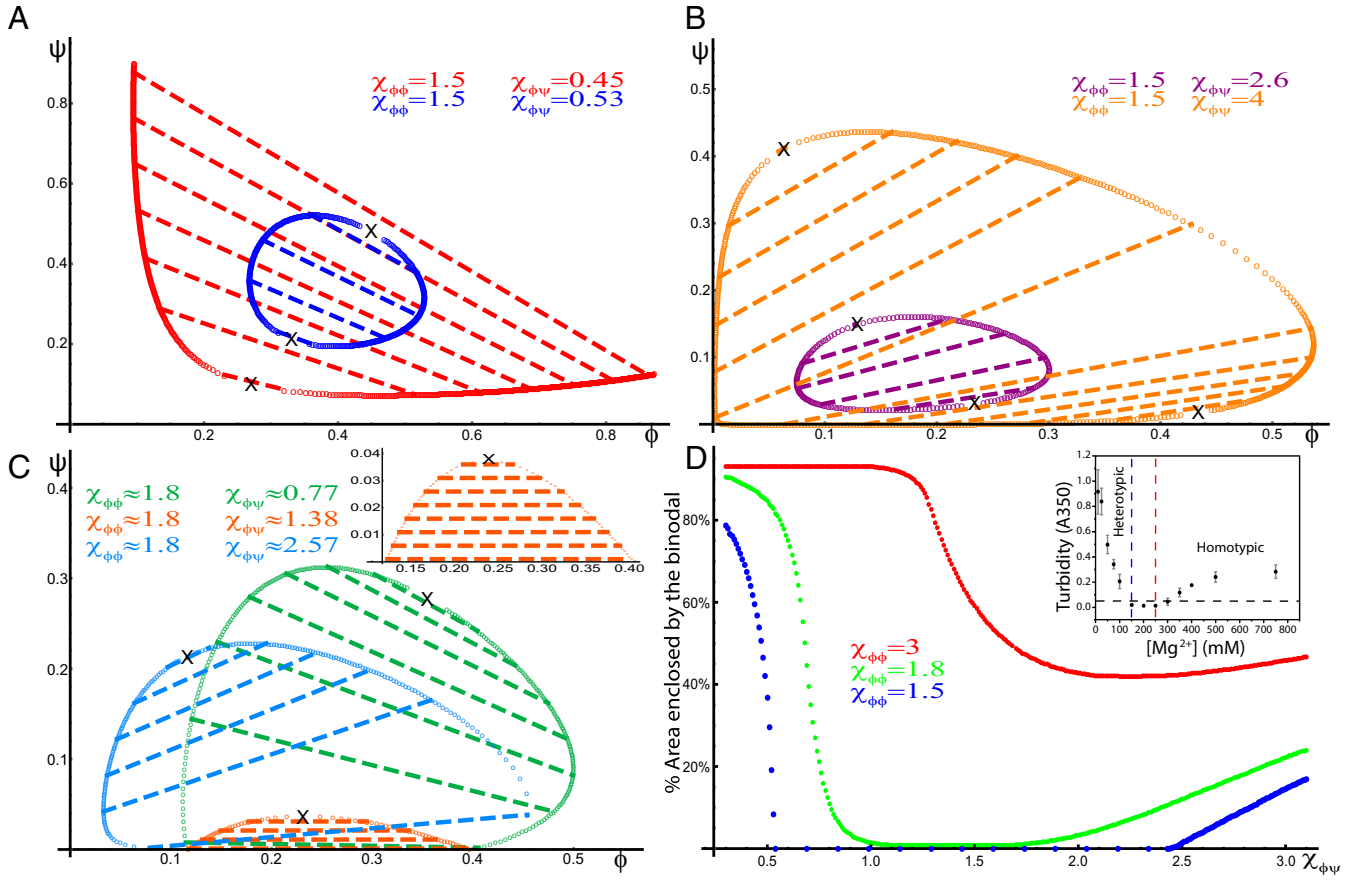

Fig. 5. Phase diagrams of ternary systems of a multivalent scaffold ϕ (with homotypic interactions) and a multivalent binding partner ψ (that heterotypically associates with the scaffold) in a solvent ($\chi_{\phi\phi}, \chi_{\phi\psi} > 0$, $\chi_{\psi\psi}=0$). Binodals are marked by open circles (that sometimes coalesce and appear as solid lines), tie-lines are marked by dashed lines, and critical points are marked by X. (*A* and *B*) Phase diagrams for $N_\phi = 10$, $N_\psi = 8$, and $\chi_{\phi\phi} = 1.5$ (smaller than $\chi^c_{\phi\phi} \approx 1.73$) for four different heterotypic interactions: $\chi_{\phi\psi} = 0.45$ (red), $\chi_{\phi\psi} = 0.53$ (blue), $\chi_{\phi\psi} = 2.6$ (purple), and $\chi_{\phi\psi} = 4$ (orange). These diagrams indicate a discontinuous transition between segregative (negatively sloped tie-lines) and associative (positively sloped tie-lines) LLPS as $\chi_{\phi\psi}$ increases when $\chi_{\phi\phi} < \chi^c_{\phi\phi}$. (*C*) Phase diagrams for $N_\phi = 10$, $N_\psi = 8$, and $\chi_{\phi\phi} = 1.8$ (larger than $\chi^c_{\phi\phi} \approx 1.73$) for three different heterotypic interactions: $\chi_{\phi\psi} = 0.77$ (green), $\chi_{\phi\psi} = 1.38$ (orange), and $\chi_{\phi\psi} = 2.57$ (blue). These diagrams indicate a continuous transition between segregative and associative LLPS as $\chi_{\phi\psi}$ increases, for the case where the system phase separates in the absence of the binding partner ($\psi = 0$), $\chi_{\phi\phi} > \chi^c_{\phi\phi}$. At a characteristic heterotypic interaction $\chi^t_{\phi\psi}$ (here ≈ 1.38) (*SI Appendix*), the tie-lines are parallel to the ϕ axis, and the area enclosed by the binodal is minimal (orange and *Inset*). (*D*) A plot of the area enclosed by the binodal (as the percentage of the physically relevant area enclosed by the triangle in the phase diagram, whose vertex is at the origin and base is at the physical limits of the two concentrations, $\phi + \psi = 1$) as a function of $\chi_{\phi\psi}$ for three values of $\chi_{\phi\phi}$: $\chi_{\phi\phi} = 1.5$ (blue), $\chi_{\phi\phi} = 1.8$ (green), and $\chi_{\phi\phi} = 3$ (red). When $\chi_{\phi\phi}$ is smaller than $\chi^c_{\phi\phi}$ (blue curve), the system exhibits reentrant behavior indicated by the range of $\chi_{\phi\psi}$ for which the area enclosed by the binodal is zero. All three curves indicate a nonmonotonic dependence of the area enclosed by the binodal on $\chi_{\phi\psi}$, where the area initially decreases with increasing $\chi_{\phi\psi}$ but eventually increases with $\chi_{\phi\psi}$. This suggests that the effect of $\chi_{\phi\psi}$ on the stability of the LLPS depends on whether it results in segregative (smaller values of $\chi_{\phi\psi}$) or associative (larger values of $\chi_{\phi\psi}$) LLPS. In contrast to the trend as the heterotypic interaction $\chi_{\phi\psi}$ is increased, the trend as the homotypic interaction $\chi_{\phi\phi}$ is increased shows that the area enclosed by the binodal always increases as $\chi_{\phi\phi}$ increases, indicating that homotypic interactions always stabilize LLPS. (*Inset*) Experimental measurements of a phase-separating ternary solution consisting of a positively charged peptide and RNA in a salt buffer. The turbidity follows the trend predicted for the area of the binodal because the variation of the concentration of Mg^{+2} ions modulates the balance of homotypic and heterotypic interactions (23) and switches the type of LLPS from associative to segregative, respectively, denoted in *Inset* as "heterotypic" and "homotypic." Adapted from ref. 23.

$\chi^{lc}_{\phi\psi} < \chi_{\phi\psi} < \chi^{uc}_{\phi\psi}$, phase separation is completely inhibited, and the single-phase state of the solution dominates at all concentrations ϕ, ψ, suggesting a reentrant LLPS in the scaffold–client model as $\chi_{\phi\psi}$ increases.

In contrast, if the scaffold has strong homotypic interactions so that it does not require a crowder to undergo LLPS (*SI Appendix*, Table S2), our model predicts a continuous change of the topology of the phase diagram with no reentrant behavior. The area enclosed by the binodal decreases with increasing $\chi_{\phi\psi}$, is minimal at a particular value of $\chi_{\phi\psi} = \chi^{t}_{\phi\psi}$ (*SI Appendix*), and subsequently increases as $\chi_{\phi\psi}$ is further increased (Fig. 5 *C* and *D*). Similarly, the slopes of the tie-lines transition continuously from negative values for $\chi_{\phi\psi} < \chi^{t}_{\phi\psi}$ to positive ones for $\chi_{\phi\psi} > \chi^{t}_{\phi\psi}$; for $\chi_{\phi\psi} = \chi^{t}_{\phi\psi}$ (Fig. 5 *C*, *Inset*), the tie-lines are completely horizontal.

Discussion

There are two main differences between a binary solution and one with two or more solutes, which we explain in terms of ternary solutions containing two solutes. First, in the case of homotypically attracting solute in the presence of an additional inert solute, crowding interactions promote LLPS and also, rotate the tie-lines, which then can make concentration buffering less effective, compared with a binary solution of the homotypically attracting solute and a solvent. Second, the two solutes can undergo LLPS driven by heterotypic interactions as well as homotypic ones. For LLPS that is driven by both homotypic and heterotypic interactions, the orientation of the tie-lines may be a continuous function of the interactions. In the subsections below, we discuss the unique features of the phase diagrams of ternary systems that we predicted above, with particular emphasis on the different roles of homotypic vs. heterotypic interactions. We then relate these to their consequence on concentration buffering and review experimental observations that support our theoretical predictions.

It is important to note that we have used a mean-field theory that neglects thermal fluctuations, which themselves can contribute to variation of the concentrations within the coexisting domains. If these variations are larger than the difference between the mean-field, coexisting concentrations, then our mean-field theory becomes inadequate to describe the LLPS. However, thermal fluctuations become significant only very close to critical points (40), which are predicted by our theory in some of the concentration–concentration diagrams (marked by X in Figs. 3–5). Near these critical points, the length of the tie-lines that connect the points of coexisting concentrations approaches zero, which means that the compositions of the BMCs and their environment become very similar. Consequently, the interfacial energy of the BMCs becomes small so that their shape is expected to be highly fluctuating (14), in principle, even at the scale of their own size. Since BMCs are usually reported to be stable in shape and distinct in composition from their environment, we conclude that biological systems are usually far away from critical points, so that our theory is valid and thermal fluctuations are negligible.

Homotypic Interactions: Effect of Crowders. Our model predicts that addition of a crowder (inert macromolecule) to a homotypically phase-separating solute promotes LLPS. This results in a decrease of both the minimal homotypic interaction strength required for LLPS and the supersaturation concentration of solute for homotypic interaction energies that exceed the minimal one. Furthermore, these effects increase for larger and higher-concentration crowders (*SI Appendix* has detailed analysis). These predictions are consistent with experimental findings as reflected by the similarities of our predicted phase diagram and an experimentally measured one, adapted from ref. 38 (in Fig. 3 *A*, *Inset*, there is a sharp rise in the binodal near $\phi = 0$).

As shown in Fig. 3, our theory suggests a classification of homotypically phase-separating molecules into two types according to the topology of their phase diagram. The binodal of the first type intersects the line $\psi = 0$ (ϕ axis), where ψ is the crowder concentration and ϕ is the concentration of the phase-separating solute. Phase separation exists even when the crowder concentration is zero. The second type does not intersect this line; the phase separation only exists for finite values of the crowder concentration. This (*SI Appendix* has further quantification) is equivalent to a known experimental classification of phase-separating molecules into ones that do not require crowding to phase separate (our first type) and ones that do (our second type) (41); in *Concentration Buffering: Noise-Ellipse and Tie-Line Orientations*, we relate this classification to the concentration-buffering capabilities of these molecules.

Heterotypic Interactions: In the Absence or Together with Homotypic Ones. Our model predicts that in ternary solutions, LLPS driven by interactions that are either "purely homotypic" (Fig. 3) or "purely heterotypic" (Fig. 4) is segregative or associative, respectively (Fig. 1). In addition, we predict an important topological difference between these two cases. For purely homotypic LLPS, the binodal intersects the line describing a state with maximal solute concentration (zero solvent) at the edge of the diagram, characterized by the equation $\phi + \psi = 1$, and possibly the line $\psi = 0$ as well. In contrast, for purely heterotypic LLPS, the binodal takes the form of a closed loop that does not intersect the axes of the phase diagram. This indicates that an excess of either of the two solutes may suppress LLPS or in other words, that LLPS occurs only in a given stochiometric range. Our generic predictions for the different topologies of the phase diagrams in these two cases agree with experimental measurements of various specific systems (18, 38, 39, 42); examples are adapted from refs. 38 and 39 and shown as Figs. 3 *A*, *Inset* and 4, *Inset*, respectively.

The more intricate scenario for a multicomponent solution, in which LLPS is driven by more than one type of interaction, is explored in Case III where both homotypic ($\chi_{\phi\phi} > 0$) and heterotypic ($\chi_{\phi\psi} > 0$) interactions are present. We find that the topologies of the phase diagram and their dependence on the relative strengths of the heterotypic and homotypic interactions can be divided to three classes: 1) $\chi_{\phi\phi} > \chi^{c}_{\phi\phi}$, so that ϕ can phase separate even in a binary solution; 2) $\chi^{m}_{\phi\phi} < \chi_{\phi\phi} < \chi^{c}_{\phi\phi}$, so that ϕ can undergo either associative LLPS due to heterotypic interactions or segregative LLPS due to homotypic interactions but only when enabled by crowding interactions from the other solute ψ; and 3) $\chi_{\phi\phi} < \chi^{m}_{\phi\phi}$, so that the homotypic interactions of ϕ are too weak to drive segregative LLPS, and the only LLPS that can occur is associative LLPS driven by heterotypic interactions between ϕ and ψ. The prediction of reentrance of the LLPS as the heterotypic interaction is varied in class 2 is supported by in vitro measurements of a ternary solution containing RNA and arginine-rich peptide whose homotypic and heterotypic interactions are continuously modulated by buffer conditions (23) (Fig. 5 *D*, *Inset*; adapted from ref. 23). Furthermore, experimental measurements in multiple systems (17, 36, 43–47) demonstrate transitions between segregative and associative types of LLPS as the interaction strengths are changed by mutations or addition of multivalent binding partners. The latter may effectively change the interaction strengths (48). With this interpretation, the experimental measurements of the switch between the associative and segregative types of LLPS are consistent with the predictions of our model for classes 1 and 2.

The area of the two-phase regions as a function of the heterotypic interaction, is plotted in Fig. 5*D* for three systems of classes 1 and 2. The plots show that an increase of the homotypic interaction promotes LLPS in both segregative and associative LLPS. This is because both types of LLPS result in a

concentrated phase of the homotypically attractive solute. In contrast, the effect of changes in the heterotypic interactions generally depends on the type of LLPS. Increase of a heterotypic interaction between two solutes that phase separate associatively promotes LLPS. Conversely, LLPS that is segregative with respect to two solutes is inhibited by an increase of the heterotypic interaction between the solutes, which tends to associate them. This prediction of the potential adverse effect of multivalent binding partners on the stability of LLPS is consistent with previous simulations of multicomponent, phase-separating systems (49, 50).

Importantly, in class 1 systems, the multivalent solute ψ is not required for LLPS and is thus not considered as a scaffold (36). Nonetheless, its concentrations within the coexisting domains are determined by the phase diagram. This suggests a possible mechanism for targeting into the BMC proteins (such as enzymes) that are required for the proper function of the BMC; if these proteins include amino acid sequences that multivalently interact with the scaffolds of the BMC, their targeting into the BMC is guaranteed by the interactions that underlie its formation. Additionally, the concentrations of these targeted proteins may be buffered if certain conditions, which are discussed in the following subsection, are satisfied.

Concentration Buffering: Noise-Ellipse and Tie-Line Orientations. In *Concentration Buffering in Solutions of Two Solutes*, we explained that LLPS of multicomponent solutions can effectively buffer correlated expression noise when the noise ellipse is oriented along the direction of the tie-lines of the phase diagram. This prediction is generic and applies to all systems regardless of the molecular details of the noise and interactions leading to LLPS, as long as the timescales associated with the noise and the LLPS are well separated (as explained in detail in *SI Appendix*). To measure the effects of expression noise, the genes of the proteins of any system of interest can be edited to include two different fused fluorescent markers. The total integrated fluorescent signal of each marker within a cell is proportional to the overall protein concentration. Along with calibration curves of the chosen fluorescent markers, this allows measurements of the overall protein concentrations at different times and of different cells, so that the noise ellipses can be plotted independent of LLPS. Then, the noise ellipses can be compared with the directions of the tie-lines that connect pairs of coexisting concentrations on the phase diagram. In systems where noise is deleterious, we expect the noise ellipse and tie-lines to be more aligned compared with systems where the noise has no negative effect.

To discuss the possibility of effective concentration buffering in vivo, we distinguish between BMCs that have relatively high concentrations of only one multivalent macromolecule and those that have relatively high concentrations of more than one multivalent macromolecule. These correspond to the purely homotypic (Case I) and heterotypic (Cases II and III) situations, respectively, described above for the case of two solutes in a solvent.

In Case I, BMCs are formed by LLPS that is driven by homotypic interactions of one solute and modulated by crowding interactions. In the cellular environment, there are many types molecules that can act as crowders. Since all of these crowders do not interact heterotypically with the solute that forms the BMC, they can be treated in an averaged way as a single effective crowder. This is supported by many in vitro experiments that recapitulate in vivo crowding using a single type of macromolecule (51). However, the expression of the effective crowder results from the expression of many chemically distinct crowders, so that one does not expect any correlation between the expression of the effective single crowder and the solute that form the BMC. As a result, the noise ellipse of the concentration of the solute, ϕ, and the effective crowder, ψ, is parallel to the ϕ axis.

In contrast to the noise ellipse that is parallel to the ϕ axis, our theory predicts that the tie-lines generally are not (Fig. 3). Only in the specific case where there are no crowders ($\psi = 0$) and the homotypically attracting solute still phase separates are the tie-lines parallel to the ϕ axis (and are actually part of it). However, as the concentration of effective crowder increases, the slope of the tie-lines becomes negative. This means that the effective crowder introduces a mismatch between the direction of the noise ellipse and the directions of the tie-lines. Subsequently, the presence of the effective crowder reduces the buffering efficiency in a manner that depends on its concentration. This prediction agrees with the experimental measurements of ref. 15.

In that paper, measurements of the noise in the expression of a homotypically attracting protein in vivo showed a decrease subsequent to LLPS but to a lesser degree than predicted for binary solution. A detailed dynamic theory predicted trends of the noise reduction as a function of protein concentration but with higher efficiency than observed (figure 2D in ref. 15). However, their theory did not treat the effect of crowders, which our theory suggests may account for the reduced buffering efficiency.

If the expressions of the genes encoding the different macromolecules that comprise the BMC are regulated by common "master" molecules (e.g., transcription factors), their expression noise may be correlated, which rotates the effective noise ellipse relative to the ϕ axis (Fig. 2 *C* and *D*). We therefore consider two multivalent macromolecular solutes, a homotypically attracting solute and a heterotypic binding partner, which is not required for the LLPS of the former. In this case, our theory predicts that the slope of the tie-lines increases in a continuous manner as the heterotypic interactions are increased. This suggests that for the in vivo situation of many interacting solutes, the orientation of the tie-lines in the phase diagram changes continuously with the heterotypic interactions of these solutes. In that case, mutations of the various macromolecules that modulate their heterotypic interactions can change the orientation of the tie-lines in the phase diagrams and with it, the efficacy of concentration buffering for a given noise ellipse. We demonstrate this idea quantitatively in *SI Appendix*, Fig. S1 for a system of a multivalent scaffold and a multivalent binding partner, where the heterotypic interactions between the two are continuously varied. In this figure, we plot the mean square deviations of the solute concentrations from their mean values in the dilute phase (as a measure of biological noise) as a function of the heterotypic interactions. The plot shows that the mean square deviations and hence, the noise decrease as the tie-lines become more aligned with the direction of the noise ellipse and increase if the value of the heterotypic interaction is either larger than or smaller than this optimal value, at which alignment occurs. If the effect of the expression noise is deleterious to the organism, then mutations that decrease the angle between the noise ellipse and the tie-lines may be evolutionary selected, leading to alignment of the orientations of the noise ellipse and tie-lines over evolutionary timescales and subsequently, to more effective concentration buffering. We note that a recently investigated system provides supporting evidence for this hypothesis. The expressions of two proteins, the homotypically attracting NPM1 and its multivalent binding partner SURF6, that undergo associative LLPS to form the outer layer of the nucleolus (45) are induced by a common transcription factor, MYC (52). This suggests that the major axis of the noise ellipse is positively sloped (Fig. 2*C*) and may be aligned with the tie-lines, which are positively sloped as well (blue curve in Fig. 5*C*).

In some cases, there are regions of the phase diagrams where the tie-lines are nearly parallel to each other. This means that small variations in the overall concentrations in the direction perpendicular to the tie-lines result in only small changes to

the coexisting equilibrium concentrations. In other cases, there may be regions where the angles of the tie-lines (and hence, the equilibrium concentrations) change more sharply even for relatively small variations of the overall concentrations; this is seen as a "splay" of the tie-lines in the phase diagram. In this case, the splay of the tie-lines serves to amplify the effect of noise on the equilibrium concentrations of the coexisting phase in the side of the phase diagram where the tie-lines are maximally splayed (*SI Appendix*, Fig. S2). This then degrades the concentration buffering. On the other hand, on the opposite side of the phase diagram where the tie-lines converge, the concentrations of the equilibrium phases are even more robustly maintained even in the presence of noise. Thus, on this side of the phase diagram, the efficacy of concentration buffering may be significantly enhanced due to the proximity of the various tie-lines, even in the presence of a noise ellipse, which is not aligned with the orientation of the tie-lines (*SI Appendix*, Fig. S2). We hypothesize that such large splay may serve—in the case of phases at the side of the phase diagram where the tie-lines converge—as an additional buffering mechanism that protects essential biochemical processes from rare "catastrophic variations" of overall solute concentrations. An example of such a catastrophe is nuclear rupture, which may happen during cell migration, resulting in DNA damage and mixing of the cytoplasm and nucleoplasm (53–55). Nuclear BMCs, such as DNA repair puncta (56), may utilize splay-based buffering to make DNA repair robust to the loss of the diffusion barrier of the nuclear envelope. Future investigations that correlate the phase diagrams of BMCs with such functions are required to explore this hypothesis.

Concluding Remarks. In this paper, we formulated a theory of two solutes in a solvent to predict the generic behaviors of LLPS in multicomponent solutions in the presence of expression noise. We reached the following qualitative conclusions. 1) Crowding effects promote LLPS [which is in agreement with previous important works investigating crowding by colloids or polymers (20, 57)] but decrease its concentration buffering efficiency. 2) The effect on LLPS of heterotypic interactions between two solutes depends on whether the LLPS is segregative or associative with respect to those solutes; its effect on buffering thus depends on the overall interactions of the entire set of solutes driving the LLPS (interaction network). 3) LLPS involving a subset of the solutes may buffer concentration fluctuations of these solutes if the interaction network of the solutes reflects correlations between the concentration fluctuations. Mutations affecting intermolecular interactions may be subjected to evolutionary selection that improves concentration buffering.

The theory presented here is for two-phase equilibria of two solutes and a solvent. However, we expect the three conclusions summarized in the preceding paragraph to hold for solutions containing many solutes due to the following reasons as long the LLPS forms two phases, which is true for most biological BMCs. First, since the effect of crowders is independent of any specific chemical characteristic, a solution with many crowder types can be effectively mapped to a solution with a single crowder type, which is treated in our theory. Second, a phase diagram of LLPS of many solutes will be associative or segregative with respect to each pair. This is affected by the overall interaction network. Therefore, it is important to note that the effect on LLPS of a change of the heterotypic interaction (e.g., due to mutations) between a pair of molecules depends on the overall interaction network driving the LLPS. Third, as we explain in *SI Appendix*, in many-solute systems, noise ellipses and tie-lines can be defined in their multidimensional phase diagrams. Since the tie-lines in LLPS of many solutes always define an orientation, even in a multidimensional space, as does the major axis of the multidimensional noise ellipse, our conclusions about concentration buffering when these directions are aligned are still relevant.

Data Availability. All study data are included in the article and/or *SI Appendix*.

ACKNOWLEDGMENTS. We thank Omar Adame Arana, Gaurav Bajpai, Lucy Brennan, Guoming Gao, Hagen Hofmann, Anthony Hyman, Frank Jülicher, Gary Karpen, Adam Klosin, Emmanuel Levy, Joshua Riback, Amy Strom, and Christoph Zechner for valuable discussions. The research was supported by the Volkswagen Foundation Grant, the Weizmann–Curie Grant, the Fern and Manfred Steinfeld Professorial Chair, the Benoziyo Endowment Fund for Advancement of Science, the Henry Krenter Institute for Biomedical Imaging and Genomics, the Harold Perlman Family, and the Pearlman Grant.

1. S. F. Banani, H. O. Lee, A. A. Hyman, M. K. Rosen, Biomolecular condensates: Organizers of cellular biochemistry. *Nat. Rev. Mol. Cell Biol.* **18**, 285–298 (2017).
2. M. Feric *et al.*, Coexisting liquid phases underlie nucleolar subcompartments. *Cell* **165**, 1686–1697 (2016).
3. C. P. Brangwynne *et al.*, Germline p granules are liquid droplets that localize by controlled dissolution/condensation. *Science* **324**, 1729–1732 (2009).
4. A. Molliex *et al.*, Phase separation by low complexity domains promotes stress granule assembly and drives pathological fibrillization. *Cell* **163**, 123–133 (2015).
5. A. R. Strom *et al.*, Phase separation drives heterochromatin domain formation. *Nature* **547**, 241–245 (2017).
6. Y. Lin, D. S. Protter, M. K. Rosen, R. Parker, Formation and maturation of phase-separated liquid droplets by RNA-binding proteins. *Mol. Cell* **60**, 208–219 (2015).
7. E. Spruijt, A. H. Westphal, J. W. Borst, M. A. Cohen Stuart, J. van der Gucht, Binodal compositions of polyelectrolyte complexes. *Macromolecules* **43**, 6476–6484 (2010).
8. M. B. Elowitz, A. J. Levine, E. D. Siggia, P. S. Swain, Stochastic gene expression in a single cell. *Science* **297**, 1183–1186 (2002).
9. R. D. Dar *et al.*, Transcriptional burst frequency and burst size are equally modulated across the human genome. *Proc. Natl. Acad. Sci. U.S.A.* **109**, 17454–17459 (2012).
10. P. S. Swain, M. B. Elowitz, E. D. Siggia, Intrinsic and extrinsic contributions to stochasticity in gene expression. *Proc. Natl. Acad. Sci. U.S.A.* **99**, 12795–12800 (2002).
11. Z. Wang, J. Zhang, Impact of gene expression noise on organismal fitness and the efficacy of natural selection. *Proc. Natl. Acad. Sci. U.S.A.* **108**, E67–E76 (2011).
12. T. Stoeger, N. Battich, L. Pelkmans, Passive noise filtering by cellular compartmentalization. *Cell* **164**, 1151–1161 (2016).
13. A. S. Holehouse, R. V. Pappu, Functional implications of intracellular phase transitions. *Biochemistry* **57**, 2415–2423 (2018).
14. S. Safran, *Statistical Thermodynamics of Surfaces, Interfaces, and Membranes* (CRC Press, 2018).
15. A. Klosin *et al.*, Phase separation provides a mechanism to reduce noise in cells. *Science* **367**, 464–468 (2020).
16. J. A. Riback *et al.*, Composition-dependent thermodynamics of intracellular phase separation. *Nature* **581**, 209–214 (2020).
17. D. M. Mitrea *et al.*, Self-interaction of npm1 modulates multiple mechanisms of liquid–liquid phase separation. *Nat. Commun.* **9**, 842 (2018).
18. P. R. Banerjee, A. N. Milin, M. M. Moosa, P. L. Onuchic, A. A. Deniz, Reentrant phase transition drives dynamic substructure formation in ribonucleoprotein droplets. *Angew. Chem.* **129**, 11512–11517 (2017).
19. D. Priftis, M. Tirrell, Phase behaviour and complex coacervation of aqueous polypeptide solutions. *Soft Matter* **8**, 9396–9405 (2012).
20. R. L. Scott, The thermodynamics of high polymer solutions. V. Phase equilibria in the ternary system: Polymer 1—polymer 2—solvent. *J. Chem. Phys.* **17**, 279–284 (1949).
21. C. Hsu, J. Prausnitz, Thermodynamics of polymer compatibility in ternary systems. *Macromolecules* **7**, 320–324 (1974).
22. H. Tompa, Phase relationships in polymer solutions. *Trans. Faraday Soc.* **45**, 1142–1152 (1949).
23. P. L. Onuchic, A. N. Milin, I. Alshareedah, A. A. Deniz, P. R. Banerjee, Divalent cations can control a switch-like behavior in heterotypic and homotypic RNA coacervates. *Sci. Rep.* **9**, 12161 (2019).
24. R. Milo, R. Phillips, *Cell Biology by the Numbers* (Garland Science, 2015).
25. I. M. Lifshitz, V. V. Slyozov, The kinetics of precipitation from supersaturated solid solutions. *J. Phys. Chem. Solid.* **19**, 35–50 (1961).
26. C. A. Weber, D. Zwicker, F. Jülicher, C. F. Lee, Physics of active emulsions. *Rep. Prog. Phys.* **82**, 064601 (2019).
27. D. Zwicker, A. A. Hyman, F. Juelicher, Suppression of Ostwald ripening in active emulsions. *Phys. Rev.* **92**, 012317 (2015).
28. Y. I. Li, M. E. Cates, Non-equilibrium phase separation with reactions: A canonical model and its behaviour. *J. Stat. Mech. Theor. Exp.* **2020**, 053206 (2020).
29. J. A. Riback *et al.*, Spatially constrained transcriptional sources drive asphericity of intracellular liquids. *Biophys. J.* **120**, 278a (2021).
30. J. M. Choi, A. S. Holehouse, R. V. Pappu, Physical principles underlying the complex biology of intracellular phase transitions. *Annu. Rev. Biophys.* **49**, 107–133 (2020).

31. T. S. Harmon, A. S. Holehouse, M. K. Rosen, R. V. Pappu, Intrinsically disordered linkers determine the interplay between phase separation and gelation in multivalent proteins. *eLife* **6**, e30294 (2017).
32. H. Lehrach, D. Diamond, J. M. Wozney, H. Boedtker, RNA molecular weight determinations by gel electrophoresis under denaturing conditions, a critical reexamination. *Biochemistry* **16**, 4743–4751 (1977).
33. R. Wang, Z. G. Wang, Theory of polymer chains in poor solvent: Single-chain structure, solution thermodynamics, and θ point. *Macromolecules* **47**, 4094–4102 (2014).
34. P. G. De Gennes, *Scaling Concepts in Polymer Physics* (Cornell University Press, 1979).
35. D. Deviri, S. A. Safran, Equilibrium size distribution and phase separation of multivalent, molecular assemblies in dilute solution. *Soft Matter* **16**, 5458–5469 (2020).
36. S. F. Banani *et al.*, Compositional control of phase-separated cellular bodies. *Cell* **166**, 651–663 (2016).
37. S. K. Nandi, M. Heidenreich, E. D. Levy, S. A. Safran, Interacting multivalent molecules: Affinity and valence impact the extent and symmetry of phase separation. https://arxiv.org/abs/1910.11193 (24 October 2019).
38. L. Lemetti *et al.*, Molecular crowding facilitates assembly of spidroin-like proteins through phase separation. *Eur. Polym. J.* **112**, 539–546 (2019).
39. M. Heidenreich *et al.*, Designer protein assemblies with tunable phase diagrams in living cells. *Nat. Chem. Biol.* **16**, 939–945 (2020).
40. Z. G. Wang, Concentration fluctuation in binary polymer blends: χ parameter, spinodal and Ginzburg criterion. *J. Chem. Phys.* **117**, 481–500 (2002).
41. A. A. André, E. Spruijt, Liquid–liquid phase separation in crowded environments. *Int. J. Mol. Sci.* **21**, 5908 (2020).
42. M. R. White *et al.*, C9orf72 poly (pr) dipeptide repeats disturb biomolecular phase separation and disrupt nucleolar function. *Mol. Cell* **74**, 713–728 (2019).
43. P. Yang *et al.*, G3bp1 is a tunable switch that triggers phase separation to assemble stress granules. *Cell* **181**, 325–345 (2020).
44. D. W. Sanders *et al.*, Competing protein-RNA interaction networks control multiphase intracellular organization. *Cell* **181**, 306–324 (2020).
45. M. C. Ferrolino, D. M. Mitrea, J. R. Michael, R. W. Kriwacki, Compositional adaptability in npm1-surf6 scaffolding networks enabled by dynamic switching of phase separation mechanisms. *Nat. Commun.* **9**, 5064 (2018).
46. J. Guillén-Boixet *et al.*, RNA-induced conformational switching and clustering of g3bp drive stress granule assembly by condensation. *Cell* **181**, 346–361 (2020).
47. J. Wang *et al.*, A molecular grammar governing the driving forces for phase separation of prion-like RNA binding proteins. *Cell* **174**, 688–699 (2018).
48. K. M. Ruff, F. Dar, R. V. Pappu, Ligand effects on phase separation of multivalent macromolecules. *Proc. Natl. Acad. Sci. U.S.A.* **118**, e2017184118 (2021).
49. J. R. Espinosa *et al.*, Liquid network connectivity regulates the stability and composition of biomolecular condensates with many components. *Proc. Natl. Acad. Sci. U.S.A.* **117**, 13238–13247 (2020).
50. J. A. Joseph *et al.*, Thermodynamics and kinetics of phase separation of protein-RNA mixtures by a minimal model. *Biophys. J.* **120**, P1219–P1230 (2021).
51. G. Rivas, A. P. Minton, Macromolecular crowding in vitro, in vivo, and in between. *Trends Biochem. Sci.* **41**, 970–981 (2016).
52. E. K. Herter "Characterization of direct Myc target genes in *Drosophila melanogaster* and investigating the interaction of Chinmo and Myc," doctoral thesis, Julius Maximilians Universität Würzburg, Würzburg, Germany (2015).
53. D. Deviri, D. E. Discher, S. A. Safran, Rupture dynamics and chromatin herniation in deformed nuclei. *Biophys. J.* **113**, 1060–1071 (2017).
54. C. R. Pfeifer *et al.*, Constricted migration increases DNA damage and independently represses cell cycle. *Mol. Biol. Cell* **29**, 1948–1962 (2018).
55. D. Deviri *et al.*, Scaling laws indicate distinct nucleation mechanisms of holes in the nuclear lamina. *Nat. Phys.* **15**, 823–829 (2019).
56. A. R. Strom, C. P. Brangwynne, The liquid nucleome–phase transitions in the nucleus at a glance. *J. Cell Sci.* **132**, jcs235093 (2019).
57. H. N. Lekkerkerker, W. K. Poon, P. N. Pusey, A. Stroobants, P. Warren, Phase behaviour of colloid+ polymer mixtures. *Europhys. Lett.* **20**, 559 (1992).